

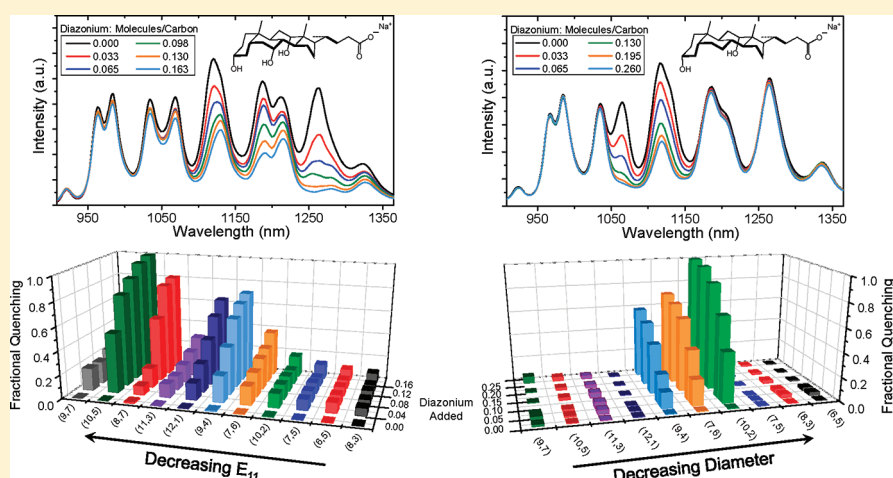
Role of Adsorbed Surfactant in the Reaction of Aryl Diazonium Salts with Single-Walled Carbon Nanotubes

Andrew J. Hilmer,[†] Thomas P. McNicholas,[†] Shangchao Lin,^{†,‡} Jingqing Zhang,[†] Qing Hua Wang,[†] Jonathan D. Mendenhall,[†] Changsik Song,[§] Daniel A. Heller,[†] Paul W. Barone,[†] Daniel Blankschtein,[†] and Michael S. Strano*,[†]

[†]Department of Chemical Engineering, and [‡]Department of Mechanical Engineering, Massachusetts Institute of Technology, Cambridge, Massachusetts 02139, United States

[§]Department of Chemistry, Sungkyunkwan University, Suwon, Gyeonggi-do 440-746, Korea

Supporting Information



ABSTRACT: Because covalent chemistry can diminish the optical and electronic properties of single-walled carbon nanotubes (SWCNTs), there is significant interest in developing methods of controllably functionalizing the nanotube sidewall. To date, most attempts at obtaining such control have focused on reaction stoichiometry or strength of oxidative treatment. Here, we examine the role of surfactants in the chemical modification of single-walled carbon nanotubes with aryl diazonium salts. The adsorbed surfactant layer is shown to affect the diazonium derivatization of carbon nanotubes in several ways, including electrostatic attraction or repulsion, steric exclusion, and direct chemical modification of the diazonium reactant. Electrostatic effects are most pronounced in the cases of anionic sodium dodecyl sulfate and cationic cetyltrimethylammonium bromide, where differences in surfactant charge can significantly affect the ability of the diazonium ion to access the SWCNT surface. For bile salt surfactants, with the exception of sodium cholate, we find that the surfactant wraps tightly enough such that exclusion effects are dominant. Here, sodium taurocholate exhibits almost no reactivity under the explored reaction conditions, while for sodium deoxycholate and sodium taurodeoxycholate, we show that the greatest extent of reaction is observed among a small population of nanotube species, with diameters between 0.88 and 0.92 nm. The anomalous reaction of nanotubes in this diameter range seems to imply that the surfactant is less effective at coating these species, resulting in a reduced surface coverage on the nanotube. Contrary to the other bile salts studied, sodium cholate enables high selectivity toward metallic species and small band gap semiconductors, which is attributed to surfactant-diazonium coupling to form highly reactive diazoesters. Further, it is found that the rigidity of anionic surfactants can significantly influence the ability of the surfactant layer to stabilize the diazonium ion near the nanotube surface. Such Coulombic and surfactant packing effects offer promise toward employing surfactants to controllably functionalize carbon nanotubes.

INTRODUCTION

Covalently modified carbon nanotubes have been utilized for a variety of applications,¹ ranging from drug-delivery vehicles^{2–4} to molecular sensors,^{5,6} and are promising materials for the development of both optical⁷ and mechanical⁸ switches. However, for such applications as electronic sensors and

actuators, the introduction of covalent defect sites to the highly conjugated nanotube sidewall significantly alters the electronic

Received: October 17, 2011

Revised: December 2, 2011

Published: December 5, 2011

properties of the nanotube, which in the case of single-walled carbon nanotubes (SWCNTs) can substantially hinder tube conductance.^{9,10} Additionally, in the case of semiconducting SWCNTs, such defect sites can quench nanotube fluorescence along a length of approximately 140–240 nm,^{11,12} thereby inhibiting the use of covalently modified nanotubes for fluorescence sensing applications. Thus, there is interest in developing a means of controlling the degree of covalent functionalization, such that the majority of the properties of pristine nanotubes are preserved.

To date, efforts toward controlling the extent of nanotube reaction have primarily focused on reaction stoichiometry,¹³ reaction time,¹⁴ and harshness of oxidative treatment.^{15–17} However, nanotube solutions may possess as many as 30 distinct species of semiconducting nanotubes alone,¹⁸ with each nanotube potentially exhibiting a significantly different affinity toward a reagent molecule. In fact, the reactivity of a particular species is often dependent upon the specific properties of the nanotube,¹⁹ including electronic structure,^{20–22} diameter,¹⁷ and bond curvature radius.²³ Therefore, it remains difficult to obtain similar degrees of functionalization across all species. Here, we examine the promise of utilizing dispersing agents to help control the extent of functionalization in the reactions of carbon nanotubes with diazonium salts.

Diazonium salts are useful candidates for the covalent modification of carbon nanotubes because they can be synthesized with a variety of different functional groups,²⁴ which can then be utilized for additional chemistry.^{25,26} However, it is well-known that aryl diazonium salts undergo a large number of reactions in solution.²⁷ Even in the limited case of aryl diazonium reactions with carbon nanotubes, a variety of mechanisms have been proposed,^{21,28–30} sometimes displaying significantly different trends in reaction selectivity. These trends range from enhanced reactivity of metallic, and large diameter species,^{21,31} to preferential reaction of small bandgap tubes.²⁸ In the case of a metallic-selective reaction, it has been determined that the rate-limiting step of the reaction involves electron-transfer from the nanotube to the diazo moiety and that selectivity is imparted during the initial adsorption step of the reaction.^{21,31} This has allowed for the use of chemical derivatization as a means of separating carbon nanotubes by electronic type^{32,33} and for increasing the on-off ratio of SWCNT network transistors.^{34–36} In the small band gap selective case, the trend in reactivity has been attributed to the formation of an electron-rich, diazoanhydride intermediate under basic conditions. However, despite these mechanistic hypotheses, little work has been expended toward elucidating the role of the surfactant in these reactions.

Because surfactants and polymers stabilize nanoparticles by a variety of mechanisms, from Coulombic forces to steric exclusion and thermal fluctuations,³⁷ it should be expected that these adsorbed layers will also influence the ability of a reagent molecule to access the nanoparticle surface. It is useful to explore this effect for two reasons: (1) the reactions of SWCNT–surfactant complexes can provide insight into the structure of the surfactant wrapping and (2) the surfactant wrapping, if understood, can help direct and control the chemical functionalization of SWCNTs, as we show. Indeed, promise toward utilizing surfactants to direct SWCNT modification has been demonstrated in the regioselective end-modification of oxidized carbon nanotubes.^{38–40} Here, we investigate the influence of surfactant on the diazonium reactions of carbon nanotubes. We particularly focus on the

fluorescence quenching response of SWCNT solutions, since this provides the most sensitive indicator of covalent functionalization.²⁸ In doing so, we design the reaction conditions such that there is only a partial quenching of the nanotube fluorescence, since these conditions are likely to correspond to the case in which the nanotubes possess both pristine segments and covalent functional handles. Ultimately, it is found that the surfactant can affect the reactions of carbon nanotubes in a variety of ways, including electrostatics, steric exclusion, and direct chemical modification of the reacting species.

METHODS

Sample Preparation. HiPCO nanotubes (Unidym, Inc.) were suspended using methods similar to those previously published,⁴¹ which have been shown to produce individually dispersed carbon nanotubes, thereby minimizing aggregation effects. Briefly, for each sample, nanotubes were dispersed at 1 mg of SWCNT/mL solution (~30 mL total volume) via 30 min of homogenization using a T-10 Ultra-Turrax (IKA Works, Inc.) dispersion element at approximately 11 400 min⁻¹. Linear chain surfactants were utilized at 1 wt %, whereas bile salts were used at a concentration of 2 wt %. The homogenized dispersions were sonicated at 10W and 0 °C for 1 h using a 6 mm probe tip (Cole-Parmer). Samples were then centrifuged at 30 000 rpm (153 720 rcf) and 22 °C for 4 h, and the supernatant collected. For CTAB, efforts were made to minimize the precipitation of surfactant during ultracentrifugation by operating above the Krafft temperature ($T_{\text{Krafft}} \sim 25$ °C). The aryl diazonium salt, 4-Propargyloxybenzenediazonium tetrafluoroborate, was synthesized according to previous protocols^{26,42,43} and stored at –20 °C until use. Fresh stock solutions of diazonium were prepared immediately prior to all experiments.

SDS and CTAB Transient Reactions. SWCNT solutions (pH 5) were preheated to 45 °C and the PL was allowed to stabilize for 1 h prior to initiating the reaction. Reactions were initiated by a single injection of diazonium solution to the well-stirred vessel, such that the final molar ratios of diazonium to carbon were 1.10×10^{-4} and 3.25×10^{-2} for SDS and CTAB, respectively. Photoluminescence spectra were obtained using a fiber optically coupled MKII Probe Head (Kaiser Optical Systems), fitted with an immersion optic, which served as both the excitation and collection device. The excitation element of the probe head was fiber optically coupled to a 785 nm Kaiser Invictus laser (~54 mW at sample). The collection port was coupled to a liquid-nitrogen-cooled nIR InGaAs detector (Princeton Instruments) through a PI Acton SP2150 spectrometer, with which transient photoluminescence spectra were acquired.

SDS Selective Reaction. SDS selective reactions were carried out by preheating samples (pH 5) to 45 °C, allowing them to stabilize at that temperature, and initiating the reaction by a single addition of diazonium solution to the well-stirred vessel. Solutions were allowed to react for 24 h and were carried out at three different molar ratios of diazonium to carbon: 6.50×10^{-5} , 1.30×10^{-4} , and 1.95×10^{-4} .

Bile-Salt SWCNT Reactions. Solutions were preheated to 45 °C and allowed to stabilize for 1 h prior to addition of diazonium reagent. For all samples, the SWCNT solution was diluted to a total carbon concentration of 15 mg/L. Reactions were initiated by a single addition of diazonium solution and were allowed to proceed for 24 h at 45 °C under constant stirring. Photoluminescence (785 nm excitation) and 2D excitation–emission data were acquired using a home-built near-infrared fluorescence microscope which has been described previously.⁴⁴ Raman spectroscopy was performed on dispersed nanotube samples using a LabRAM HR spectrometer (Horiba) with a 633 nm excitation source. A Shimadzu UV-310PC spectrometer was utilized for UV-vis-nIR absorbance measurements.

Molecular Dynamics Simulations. Molecular dynamics (MD) simulations of diazonium salt adsorption to the SWCNT–surfactant complex in aqueous solution were carried out using the GROMACS 4.0 software package.⁴⁵ The SWCNT was first covered with surfactant

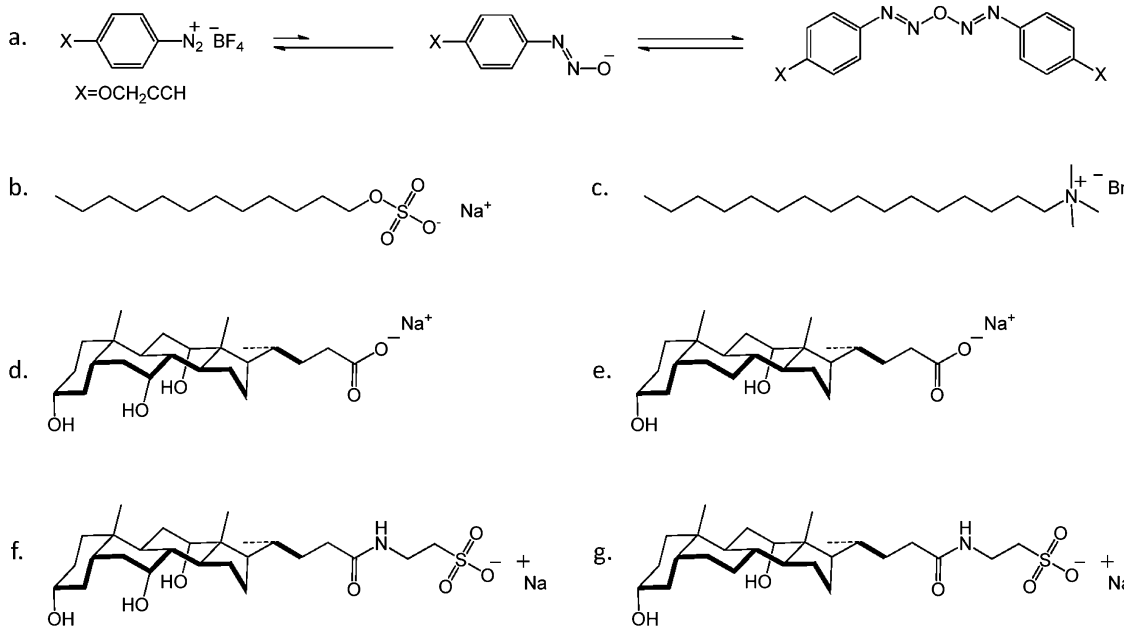


Figure 1. Structures of the diazonium ion and six surfactants utilized in this study. Diazonium salt: (a) running reactions under slightly acidic conditions favors the cationic diazonium ion over the base-mediated conversion to diazotates and diazoanhydrides. Surfactants: (b) sodium dodecyl sulfate, (c) cetyltrimethylammonium bromide, (d) sodium cholate, (e) sodium deoxycholate, (f) sodium taurocholate, and (g) sodium taurodeoxycholate. The bile salts (d–g) have rigid steroidal backbones, which impart them with hydrophobic and hydrophilic “faces”. The rigidity of these bile salts causes them to form close-packed structures on the nanotube surface. The linear chain surfactants—(b) sodium dodecylsulfate and (c) cetyltrimethylammonium bromide—possess less rigid lipidic chains, which tend to coat the nanotube in a more disordered manner.

(SC or SDS), which was fully dissociated into anions and sodium counterions. These equilibrated molecular configurations were obtained using the same simulation method described in a recent simulation work for the SC–SWCNT assembly.⁴⁶ The simulation parameters used in the present study and the force field parameters for water, SWCNT, and SC were also drawn from ref 46. Note that a thermostat of 45 °C was applied for all of the simulations to match experimental conditions. The alkane tail of SDS was modeled using the OPLS-AA force-field,⁴⁷ with updated dihedral parameters.⁴⁸ The sulfate head of SDS and its connection to the dodecyl tail were modeled following Lopes et al.⁴⁹ The surface coverage of SC and SDS were chosen to be the same (1.4 molecules/nm²) in order to rule out the long-range electrostatic effects resulting from surface charge densities to the adsorption (or binding) affinity of the diazonium ion.

The tetrafluoroborate anion (BF_4^-) of the diazonium salt was modeled using the force field parameters in ref 49. The atomic charges of the diazonium ion were not previously available in the literature and were generated here using the ab initio quantum-mechanics software package, Gaussian 03,⁵⁰ together with the CHELPG electrostatic potential-fitting algorithm⁵¹ at the MP2/cc-pVTZ(-f)/HF/6-31G* level of theory. This level of theory was selected for the purpose of maintaining consistency with the models of Lopes et al.^{49,52,53} The cc-pVTZ(-f) basis set was adapted from the cc-pVTZ basis set of Dunning,⁵⁴ as provided at the Basis Set Exchange,^{55,56} by removing the d polarization function from hydrogen and f polarization functions from heavier atoms.⁵² All other force field parameters for the diazonium ion were drawn from the OPLS-AA force field.

The interaction between the diazonium ion and the SWCNT–surfactant complex was quantified using the potential of mean force (PMF) calculation. To mimic the extremely low diazonium salt concentration in the experiment, only one diazonium ion was introduced in the simulation cell. It was constrained at various radial positions, r , relative to the cylindrical axis (z axis) of the SWCNT, and allowed to move freely on each concentric cylindrical surface around the nanotube. Each simulation was equilibrated for 10 ns before recording the mean force (averaged over another 10 ns), $\langle f(r) \rangle$, which is required to constrain the diazonium ion at each r value. The PMF (or the Gibbs free energy of the diazonium ion), as a function of r , was

obtained by numerically integrating $\langle f(r) \rangle$ along r , specifically

$$\text{PMF}(r) = \int_d^r \langle f(r) \rangle \, dr + k_B T \ln(r/d) \quad (1)$$

where d is the largest separation distance along r , k_B is the Boltzmann's constant, and $T = 45$ °C is the temperature. Note that $k_B T \ln(r/d)$ accounts for the entropy loss of the diazonium ion as a result of decreasing the area of the concentric surface from $2\pi dL$ to $2\pi rL$, where L is the length of the simulated SWCNT.

RESULTS

In order to study the influence of surfactants on the diazonium derivatization of carbon nanotubes, six surfactant molecules were utilized (Figure 1). For examining the effects of surfactant charge, two linear-chain surfactants were used: sodium dodecyl sulfate (SDS) and cetyltrimethylammonium bromide (CTAB). These surfactants are expected to form loosely packed, beaded structures on the nanotube surface,^{29,57–59} which results from a tendency of the flexible aliphatic chains to orient themselves into hydrophobic regions. Further, because the molecules are not rigid, they present little steric impedance to diazonium derivatization, thereby allowing for direct observation of Coulombic effects. For examining the effects of structural packing and surfactant rigidity, four bile salts—sodium cholate (SC), sodium deoxycholate (SDC), sodium taurocholate (STC), and sodium taurodeoxycholate (STDC)—were used. In contrast to the linear-chain surfactants, these bile salts possess stiff steroidal backbones that impart them with their characteristic hydrophobic and hydrophilic “faces”.⁶⁰ Computational simulations have shown that this bifacial nature of sodium cholate causes the surfactant to form a tightly packed monolayer on the SWCNT surface.^{29,46} Therefore, these six surfactants allow for the examination of how rigidity and charge influence the reactions of diazonium salts with carbon nanotubes. It should be noted that for all reactions, the use

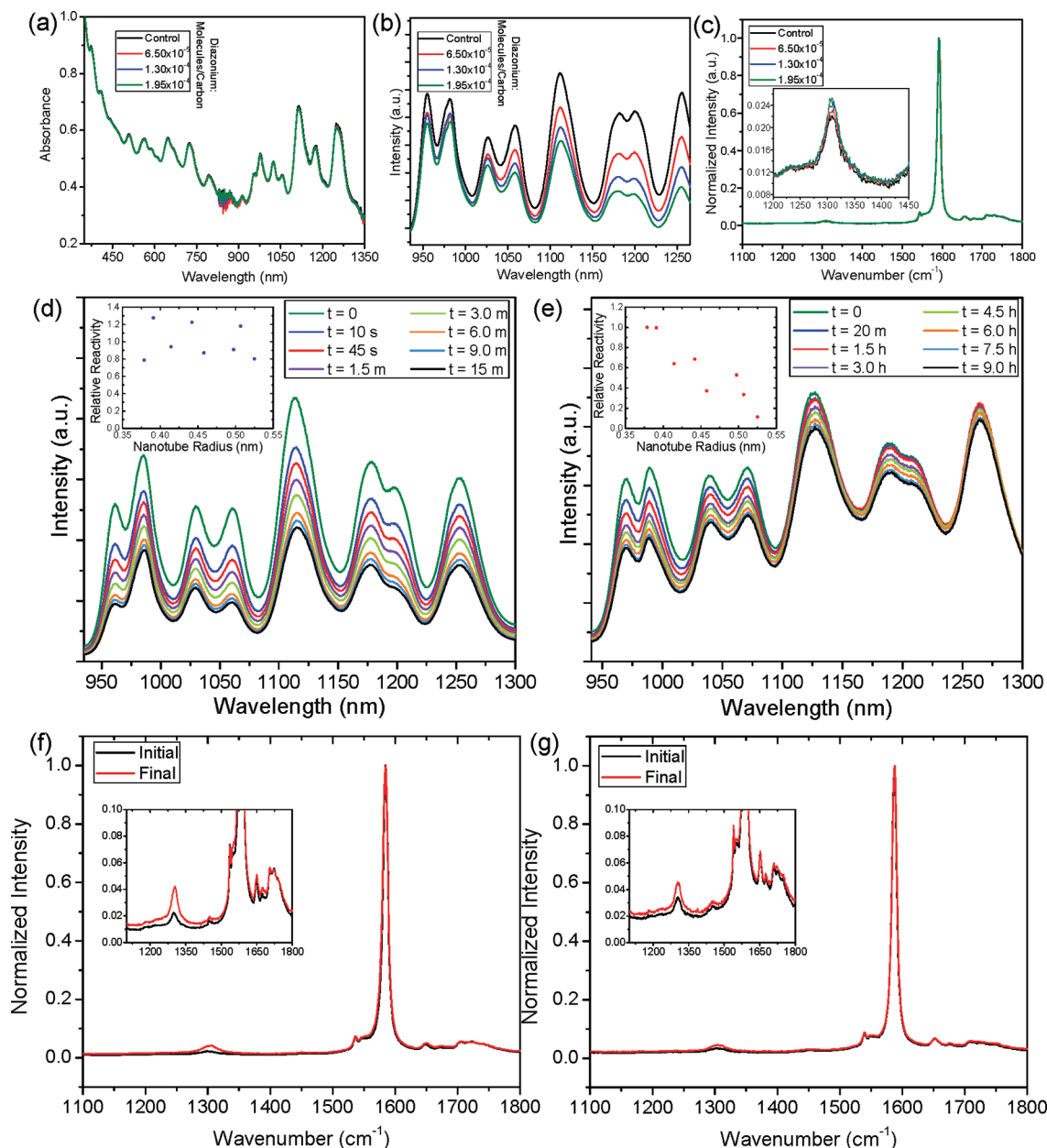


Figure 2. Reaction data for SDS and CTAB–SWCNTs under various conditions. (a–c) Selective reaction data for SDS–SWCNTs under dark conditions. (a) Absorbance data shows little change under addition of small quantities of reagent. (b) Fluorescence spectra show an enhanced reactivity of small band gap semiconductors for all aliquot sizes. (c) Raman data (normalized by the G-peak intensity) depicting slight increases in the D to G ratio with additional reagent, which is characteristic of covalent derivatization. (d and e) In situ snapshots of the transient fluorescence quenching response of carbon nanotubes suspended in (d) SDS and (e) CTAB, upon addition of diazonium salt. Here the samples are continuously illuminated at an excitation wavelength of 785 nm. (d) In the case of SDS, a similar fluorescence response is observed across all species. (e) CTAB exhibits a preferential reaction of small diameter species. Insets depict the relative reactivities of 8 nanotube species as a function of tube radius. (f and g) G-peak-normalized pre- and postreaction Raman spectra (633 nm excitation) for (f) SDS and (g) CTAB–SWCNTs, which demonstrate an enhanced D/G ratio (D peaks shown in insets).

of slightly acidic conditions aids in preserving the cationic, aryl diazonium moiety by suppressing the base-mediated conversion to the corresponding diazotate or diazoanhydride (Figure 1a).²⁷

Linear Chain Surfactants. Because the diazonium ion is cationic, it is of interest to see how the charge of the surfactant–SWCNT complex affects the ability of the diazonium molecule to access the SWCNT surface. Because of the relatively fast reaction kinetics of SDS–SWCNTs (Figure S1) and the desire to directly observe how the charge

of the SWCNT–surfactant complex actively attracts or repels diazonium ions, we continuously probed the fluorescence quenching response of SDS- and CTAB-suspended SWCNTs upon exposure to aryl diazonium salt. Under dark reaction conditions at pH 5 and $T = 45^\circ\text{C}$, SDS-suspended carbon nanotubes have been shown to undergo an electronically selective reaction which depends upon the nanotube density of states.^{21,31} Such reactions are shown in Figure 2a–c for different molar ratios of diazonium to carbon. Here, the extent of reaction is small enough that there is a negligible effect on

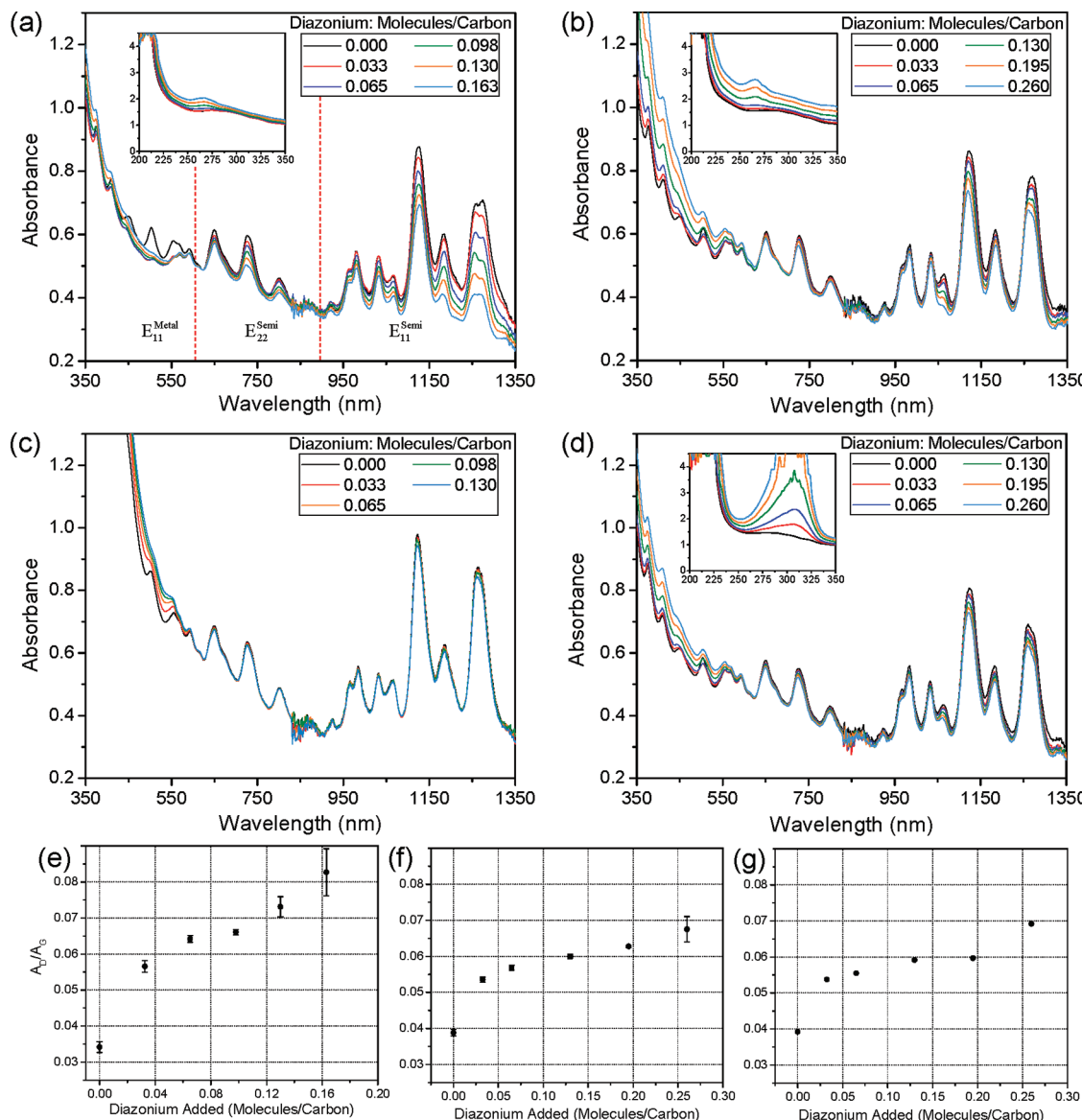


Figure 3. Absorbance spectra for four bile salts, (a) sodium cholate, (b) sodium deoxycholate, (c) sodium taurocholate, and (d) sodium taurodeoxycholate, and Raman D/G ratios for (e) sodium cholate, (f) sodium deoxycholate, and (g) sodium taurodeoxycholate. Spectra have been normalized to match $\text{abs}(632 \text{ nm})$ of the control. (a) Sodium cholate provides the clearest demonstration of selective reaction, with metallic and large diameter (small bandgap) nanotubes reacting preferentially. The other three species also appear to demonstrate an enhanced reactivity of small band gap semiconductors, albeit to different extents. The increase in baseline, toward the ultraviolet region, can be attributed to reaction byproducts. Raman reaction trends for sodium deoxycholate (f) and sodium taurodeoxycholate (g) appear similar, which is consistent with their absorbance spectra, which also show similar results. (e) The D/G ratios for sodium cholate attain higher values than those observed for the other bile salts, which is consistent with a greater decrease in the absorbance associated with Van Hove singularities.

the absorbance spectra of the solutions. In contrast, the nanotube fluorescence, which is more sensitive to covalent functionalization than absorbance,²⁸ depicts a preferential decrease in emission features associated with small band gap semiconducting nanotubes, whose E_{11} transition energies appear furthest into the near-infrared (Figure 2b). It is worth noting that SDS-SWCNTs are much more reactive than SWCNTs dispersed in other surfactants, such that a similar quantity diazonium, when applied to the other SWCNT-surfactant systems studied here, results in little to no degree of functionalization (Figure S5). This is likely attributable to both the charge and loose structural packing of the SDS molecules.

When laser-illumination is used to analyze the transient quenching response, a substantially different reaction trend is

observed for both SDS and CTAB-SWCNT solutions. For transient experiments, SWCNT suspensions (pH 5) were preheated to 45 °C and reactions were initiated by a single injection of diazonium solution. During reaction, the transient fluorescence behavior was monitored *in situ* by utilizing an immersion optic-fitted Kaiser Raman MKII probe head, which was coupled to a nIR spectrometer. In order to collect photoluminescence spectra in real time, the reacting samples were continuously excited using 785 nm laser illumination (~54 mW at sample) during the experiment. The fluorescence spectra of the SDS- and CTAB-SWCNT solutions at various time points after addition of diazonium ions are depicted in Figure 2, panels d and e, respectively. For anionic SDS, the fluorescence quenching response appears to be relatively

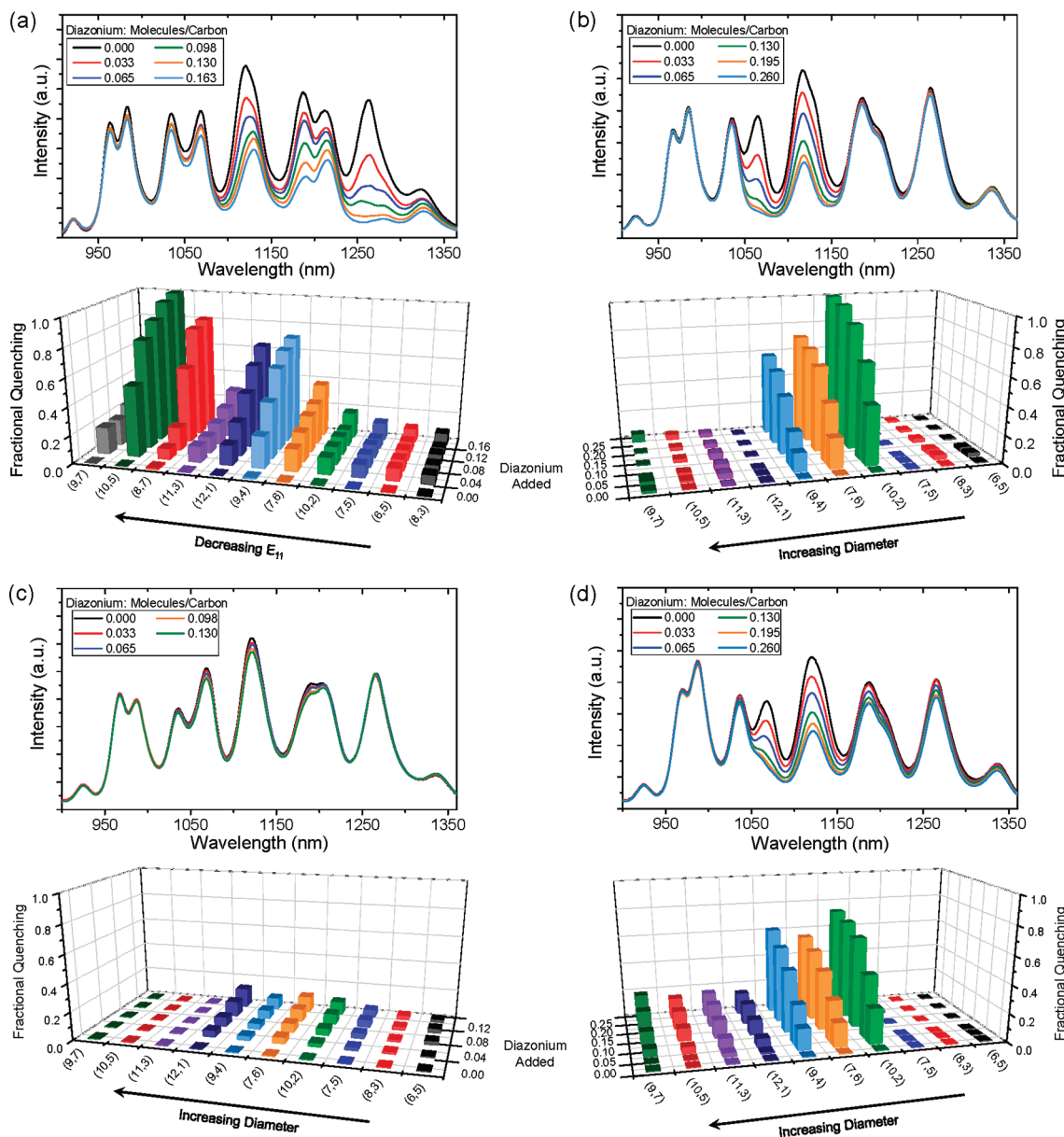


Figure 4. Fluorescence spectra and deconvoluted fractional quenching results for the four bile salts used in this study, (a) sodium cholate, (b) sodium deoxycholate, (c) sodium taurocholate, and (d) sodium taurodeoxycholate, at an excitation wavelength of 785 nm. (a) As observed in the absorbance spectra, sodium cholate demonstrates a predominantly electron-transfer selective reaction, with large diameter (small bandgap) nanotubes reacting preferentially. For sodium cholate, the fractional quenching results are generally plotted from large to small E_{11} gap. For species whose E_{11} emissions overlap to the extent that a single peak is observed (i.e., (9,4)/(7,6) and (10,5)/(8,7)), the species with the larger E_{22} gap has been plotted first. In contrast to sodium cholate, the other three bile salts display preferential reactivity among a small population of nanotubes (see text).

independent of the nanotube species, with all SWCNTs exhibiting similar degrees of quenching. Further, the quenching response occurs very quickly, leveling off after approximately 25 minutes (see Figure S1). On the other hand, CTAB–SWCNTs, besides displaying a much slower quenching rate than that of SDS-suspended nanotubes, exhibit an enhanced reactivity of large band gap (small diameter) species. Spectral deconvolution (Supporting Information) allows for more rigorous analysis of eight nanotube species whose fluorescence is predominantly observed at 785 nm laser excitation. The relative reactivities of these 8 species are depicted as a function of tube radius in the insets of panels d and e in Figure 2. In the case of both surfactant systems, covalent derivatization was

confirmed by Raman spectroscopy, which displayed an increase in the D/G ratio (Figure 2, panels f and g).

Bile Salt Derivatives. The effects of surfactant rigidity and structure were analyzed with a focus on bile salt derivatives. Here, the rigidity of the surfactant layer resulted in much slower reaction kinetics, which were dominated by the effects of structural packing, even under laser illumination (Figure S2). Therefore, for analyzing the reactions of bile salt-suspended SWCNTs, reactions were performed over a 24 h time period in the absence of illumination. The absorbance spectra of nanotube suspensions at varying conversions are depicted in Figure 3. As can be seen in Figure 3a, sodium cholate–SWCNTs appear to undergo an electron-transfer-selective

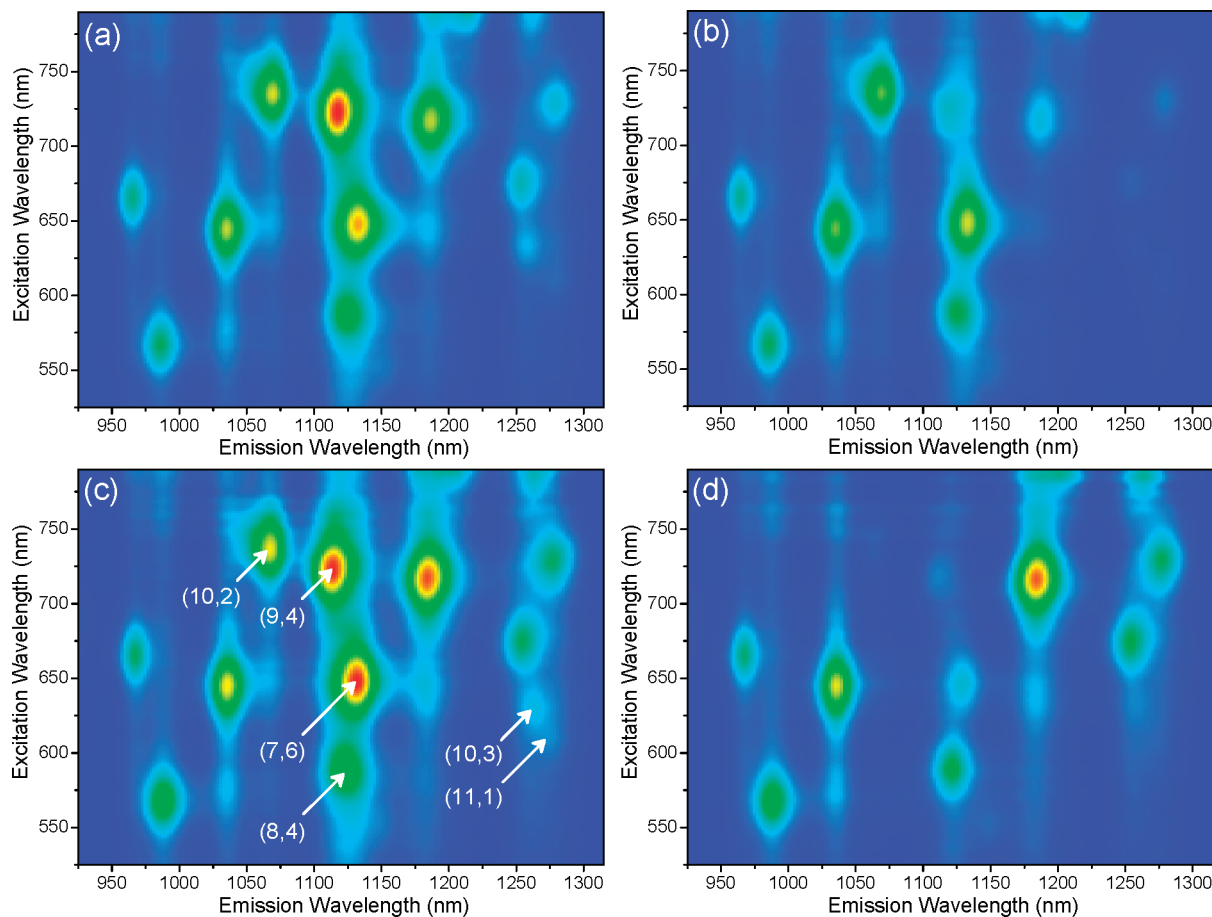


Figure 5. 2D excitation–emission spectra of unreacted (left) and reacted (right) SC–SWCNT (a and b) and SDC–SWCNT (c and d). In agreement with electron-transfer limitation, the SC–SWCNT reaction progresses from the top right to the bottom left of the plotted spectrum. SDC, however, displays reaction among predominantly a small diameter range of species, including (10,2), (9,4), (7,6), (10,3), (11,1), and, to a lesser extent, (8,4).

reaction, with peaks attributable to the metallic E_{11} transitions disappearing first, followed by small band gap and then larger band gap semiconductors. In contrast to sodium cholate, the structural homologue, sodium taurocholate (Figure 3c), exhibits a minimal degree of reactivity with only a small decrease in select absorbance peaks. The deoxycholate bile salts, sodium deoxycholate (Figure 3b) and sodium taurodeoxycholate (Figure 3d), demonstrate similar reactivity trends. However, a strong absorption peak at 309 nm, in the case of STDC-SWCNT, indicates that a significant amount of residual diazonium ion remains in the STDC-SWCNT solution, which does not appear in the case of SDC. A similar comparison between SC and STC was not possible due to saturation of the STC absorbance spectrum in the ultraviolet region. After the allotted reaction time, Raman spectra were taken in order to evaluate the D/G ratio of each sample (Figure 3e and f). Consistent with absorbance results, sodium cholate-suspended nanotubes exhibit the largest D/G ratios (Figure 3e). The two deoxycholic species, SDC (Figure 3f) and STDC (Figure 3g), appear to attain comparable D/G ratios for similar quantities of added diazonium. Raman analysis of the sodium taurocholate derivative was not possible due to a large background signal (see Figure S2). Judging from these data, it appears that all solutions have similar reactivity trends, with larger band gap species reacting preferentially to smaller band gap tubes, albeit to different extents. However, upon analyzing fluorescence data, a significantly different trend is observed.

The corresponding fluorescence spectra for the bile salt suspensions are shown in Figure 4. Here, the data are presented as both the raw spectra and deconvoluted, fractional quenching results for individual species. In agreement with the absorbance data of Figure 3, SC–SWCNTs undergo a reaction that is predominantly determined by the electronic structure of the nanotube. This is apparent from the fractional quenching results of the individual species, which have generally been arranged according to the magnitude of their E_{11} band gap. In going from right to left, those species whose E_{11} gaps overlap, such that their combined emissions appear as a single peak in the emission spectra (i.e., (9,4)/(7,6) and (10,5)/(8,7)), the species with the larger E_{22} gap has been plotted first. Here, except in the case of the (11,3) and (9,7) species, a general increase in reactivity is observed as the E_{11} band gap decreases. However, as is especially evident in the case of SDC, the other SWCNT–surfactant complexes appear to undergo reactions among only a small subset of nanotube species. For SDC–SWCNT, the reacting population is comprised of: (10,2), (9,4), (7,6), (10,3), (11,1), and, to a lesser extent, (8,4). This result is more clearly demonstrated in the 2D excitation–emission spectra of reacted and unreacted samples (Figure 5). Of these affected species, fluorescence features associated with the (10,2), (9,4) and (7,6) nanotubes are predominantly observed at an excitation wavelength of 785 nm, and their fractional quenching results are depicted in Figure 4b. Here, it is evident that these three species react to the near exclusion of the other

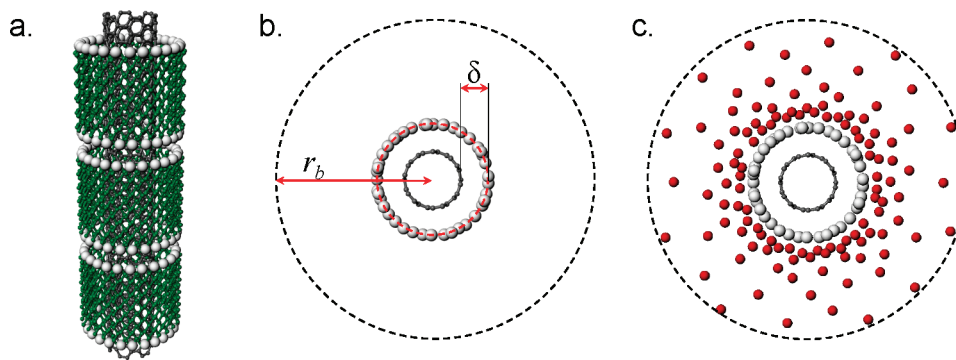


Figure 6. Illustration of the cell model, which was utilized to study the relative reactivities of SWCNTs in the diffusion limit. (a) Schematic of a surfactant encapsulated SWCNT. (b) Looking down the SWCNT axis, the charged head groups of the surfactant are assumed to reside on a cylindrical plane located a distance, δ , from the nanotube surface. The distance, r_b , is the radius at which the potential and the derivative of the potential go to zero. (c) Schematic of how the cell may appear in the presence of counterions.

semiconducting nanotubes which are observable at 785 nm excitation. Similar trends are seen for STDC (Figure 4d) and STC (Figure 4c), though to different extents of reaction. As is consistent with the absorbance data in Figure 3c, sodium taurodeoxycholate-suspended nanotubes exhibit only a small degree of fluorescence quenching when compared to the other analyzed bile salts. It is worth noting that, at even the lowest diazonium concentrations used for the bile salt species, SDS-suspended SWCNTs undergo significant extent of reaction, providing further evidence of the loose, pliable packing of SDS on the nanotube surface (Figure S6).

■ DISCUSSION

Linear Chain Surfactants: Diffusion-Limited Kinetics. Under dark conditions, SDS-SWCNTs show typical electron-transfer-limited reaction (Figure 2, panels a and b), in which metallic and small band gap species display a higher reactivity than large band gap semiconductors.^{21,32} This is consistent with reported studies in which other surfactants were utilized, including Pluronic F127³⁰ and sodium cholate,³³ and is in agreement with the predictions of electron-transfer theories.^{31,61} Generally, this selectivity results from an enhanced ability of these nanotube species to transfer an electron to the electrophilic, diazo moiety, thereby facilitating decomposition of the aryl diazonium molecule. However, under constant laser illumination, electron-transfer selectivity is not observed for either SDS or CTAB-SWCNTs. We particularly noticed that, in the case of CTAB-SWCNTs, the reaction rate was very small due to Coulombic repulsion between the diazonium ion and the adsorbed surfactant layer, giving the appearance of diffusion-limitation.

Here, a diffusion-limited model is proposed for the reaction of surfactant-coated SWCNTs with aryl diazonium salts. Each nanotube is treated as residing within a cylindrical cell of solution,^{62,63} which contains only a single SWCNT–surfactant complex and its corresponding counterions. This model hinges on the assumption that the SWCNT particles are dispersed at large enough distances that, on average, their interactions are negligible. Thus, there is a radius between SWCNTs at which the electrostatic potential goes to zero. Because nanotube solutions are typically dilute ($\sim 20\text{nM}$ in this study), this approximation should be valid. A schematic of the cell model is depicted in Figure 6. For the purpose of this study, it was assumed that the charged heads of the surfactant layer reside on a cylindrical plane located at a distance, δ , from the nanotube

surface. This distance was chosen to be 0.4 nm based on molecular dynamics simulations of SDS-encapsulated SWCNTs.⁵⁸ The distance, r_b , represents the radial distance from the SWCNT axis to the boundary of the cell, at which both the potential and the derivative of the potential go to zero.⁶⁴

In diffusion limited reactions, as in the theory of slow coagulation,⁶⁵ the rate of reaction is determined by the flux of diazonium molecules to the nanotube surface. In the presence of a potential, ψ , the flux of an ionic species is described by the Nernst–Planck equation

$$\vec{J} = -D_A \left[\nabla C_A + \frac{z_A C_A F}{RT} \nabla \psi \right] \quad (2)$$

where F is Faraday's constant and D_A , z_A , and C_A are the diffusion coefficient, charge, and concentration of the diazonium ions, respectively. If the reaction is at steady-state, and edge effects are neglected, then the number of molecules passing through a cylindrical shell of area, $A = 2\pi rL$, where L is the SWCNT length, is equal to the diazonium-SWCNT collision rate, which is given by

$$R_c = 2\pi r L D_A \left[\frac{dC_A}{dr} + C_A \frac{d(z_A F \psi / RT)}{dr} \right] = \text{constant} \quad (3)$$

Using the condition that $\lim_{r \rightarrow r_b} \psi = 0$ and assuming that the concentration of diazonium is effectively zero at the nanotube surface, it is possible to derive an expression for the rate of collision of aryl diazonium ions with a carbon nanotube in solution

$$R_c^{(n,m)} = \frac{C_\infty 2\pi L D_A}{\int_{r_{(n,m)}+\delta}^{\infty} \frac{1}{r} \exp(F\psi/RT) dr} \quad (4)$$

where C_∞ is the bulk concentration of the aryl diazonium molecule and z_A has been defined as +1. While this equation has been derived under the assumption of a constant collision rate, the ratio of collision rates, $R_c^{(n,m)}/R_c^{\text{ref}}$, fundamentally represents the relative attraction of diazonium ions to each SWCNT–surfactant complex and is therefore more generally applicable. In order to utilize this expression, it is necessary to first evaluate the potential distribution, ψ , around the nanotube.

Within the cell of our model, the potential profile can be obtained by solving a modified Poisson–Boltzmann (MPB) equation, which incorporates excluded volume effects associated with counterion condensation.^{63,66} In a micellar system in which only surfactant counterions are present, the Poisson–Boltzmann equation can be represented as

$$\nabla^2 \psi = -\frac{z_c F c_c(r)}{\epsilon} \quad (5)$$

where z_c and $c_c(r)$ are the charge and concentration of the counterion, respectively. In evaluating the potential distribution, the population of diazonium ions is neglected due to its extremely low concentration (<325 μM) relative to the surfactant (>27 mM). Accounting for excluded volume effects of ions in solution, the surfactant counterion concentration, as a function of the distance from the tube surface, can be represented by⁶⁶

$$c(r) = \frac{c_b e^{-z_c F \psi / RT}}{1 + \phi_0 (e^{-z_c F \psi / RT} - 1)} \quad (6)$$

where c_b and $\phi_0 = c_b V_{\text{ion}} N_A$ represent the concentration and volume fraction of counterions at the cell boundary, respectively. Values for V_{ion} were approximated by assuming a single hydration shell around the counterions, and utilizing hydration shell distances from the literature.^{67–70} Inserting expression 9 into eq 8 yields the modified Poisson–Boltzmann equation⁶⁶

$$\nabla^2 \psi = -\frac{z_c F}{\epsilon} \frac{c_b e^{-z_c F \psi / RT}}{1 + \phi_0 (e^{-z_c F \psi / RT} - 1)} \quad (7)$$

The boundary condition at the edge of the cell is specified by requiring that ψ and ψ' go to zero at $r = r_b$, and that at the surfactant layer is determined by evaluating Gauss' law at $r = r_{\text{SWNT}} + \delta$, with the assumption that the gradient of the potential inside of the surfactant layer is zero

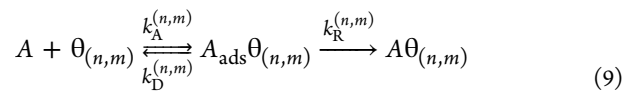
$$\left. \frac{d\psi}{dr} \right|_{r=r_{(n,m)}+\delta} = -\frac{q_e}{\epsilon}; \quad \lim_{r \rightarrow r_b} \psi, \frac{d\psi}{dr} = 0 \quad (8)$$

Here, q_e is the charge density per unit area in the surfactant layer. Using an appropriate change of variables (Supporting Information), it is possible to solve for ψ numerically, utilizing a shooting method to satisfy the boundary condition at $r = r_{(n,m)} + \delta$.

For fitting experimental data, all parameters were kept fixed except the surface coverage of surfactant, which was assumed to be invariant across nanotube species. For CTAB-suspended SWCNTs, by fitting the model to the relative reactivities of the eight nanotube species, the solid black curve in Figure 4 was obtained, which corresponds to a surface coverage of 4.3 molecules/nm². The magnitude of this value is fairly consistent with previously estimated values of 2.2–3.0 molecules/nm² for SDS suspended SWCNTs.⁷¹ The decreasing reactivity trend for CTAB–SWCNTs, as a function of tube radius, results from diameter-dependent effects and can be understood as follows. For very small nanotubes, a large cylindrical curvature exists, which results in a radially diffuse distribution of the potential associated with the surface charge density. As the radius of the tube increases, the overall charge on the tube increases, and distribution of the potential becomes less diffuse. At large enough tube radii, the potential will ultimately approach the flat

plate limit, and the relative reactivity will reach a constant value. The potential at the surface is amplified by excluded volume effects in the vicinity of the surfactant layer, which limit counterion condensation and cause the potential to reach higher values than it would in the absence of these effects. This allows the exponential term to overcome the $1/r$ dependence in the denominator of eq 4. Because the diazonium interaction with CTAB is repulsive, the inherent reaction rate is slow, and small increases in surface potential can result in noticeable changes in fluorescence quenching response.

Interestingly, if the diffusion limited model is applied to the case of SDS, the observed experimental trend is also predicted. This result can likely be attributed to the continuous excitation of SWCNT electrons during laser illumination, which serves to decrease the energy barrier for electron transfer from SWCNT to the diazonium ion. From a kinetic standpoint, the behavior can be explained as follows. The reactions of diazonium salts with carbon nanotubes proceed via a two-step mechanism in which the aryl diazonium molecule, A , first adsorbs to the SWCNT–surfactant complex and subsequently reacts with the nanotube sidewall to form a covalent bond²⁹



Here, $k_A^{(n,m)}$ and $k_D^{(n,m)}$ are adsorption and desorption rate constants, respectively, and $k_R^{(n,m)}$ is the rate of covalent reaction. Under electron-transfer limited conditions ($k_R \ll k_D$), covalent bond formation is the rate determining step, and the first step of the reaction can be assumed to be in equilibrium. This gives rise to the following kinetic expression:

$$\begin{aligned} \frac{d[A\theta_{(n,m)}]}{dt} &= \frac{k_R^{(n,m)} k_A^{(n,m)}}{k_D^{(n,m)}} [A] [\theta_{(n,m)}] \\ &= k_R^{(n,m)} K_1^{(n,m)} [A] [\theta_{(n,m)}] \end{aligned} \quad (10)$$

where $K_1^{(n,m)}$ is defined as $k_A^{(n,m)} / k_D^{(n,m)}$. For SDS–SWCNTs, if this ratio is presumed to be independent of nanotube species, then the rate constant associated with the SWCNT reaction is directly proportional to $k_R^{(n,m)}$, which is associated with electron transfer from SWCNT to the diazonium molecule. Alternatively, as is seen in this study, it is possible to decrease the activation energy associated with electron transfer by supplying excited-state electrons to the reaction. Here, this is done through constant laser excitation at 785 nm. If the rate of electron transfer is significantly enhanced (k_R becomes large), a pseudosteady-state approximation can be made on the concentration of the adsorbed intermediate. Such a treatment leads to the following kinetic expression:

$$\frac{d[A\theta_{(n,m)}]}{dt} = \frac{k_R k_A}{k_R + k_D} [A] [\theta_{(n,m)}] \quad (11)$$

In the case that $k_R \gg k_D$, the reaction appears to be equivalent to the one shown below, and the reaction is adsorption, or diffusion, limited



Because diazo groups are stable to irradiation at red wavelengths,²⁷ the increased reactivity most likely stems from excitation of electrons within the nanotube species, rather than

irradiative decomposition of the aryl diazonium moiety. It is interesting to note that in the cases of both CTAB and SDS, similar species tend to lie above or below the predicted, theoretical curves. This may be due to species-dependent differences in surfactant adsorption, where slight differences in surfactant surface coverage could alter the potential experienced by the diazonium ion. However, if the variation were adsorption-dependent, we would expect to observe a correlation with species diameter, since previous results have indicated that SDS binds more strongly to small diameter species.⁷² In the present case, the scattering in the data may more likely be attributable to differences in exciton diffusion length,⁶⁴ which would cause certain species to experience a greater degree of quenching for a similar extent of functionalization. However, due to the limited data that are currently available, it is difficult to correct for these differences. In sodium deoxycholate, there appears to be a correlation between the apparent exciton range and the diameter of the nanotube, with smaller diameter tubes displaying a shorter exciton mobility.⁶⁴ However, it is unlikely that these species-dependent values can be directly applied to the case of linear chain surfactants, since an alternative study has demonstrated that the surfactant, alone, can induce variations in exciton diffusion length.¹² Despite this, we applied a correction for exciton mobility based on the available SDC results (Figure S7). Although this correction seemed to reduce the scattering of data points at small SWCNT diameters, there was a significant deviation of the data points for larger diameter species. This is likely attributable to the influence of the surfactant on the exciton diffusion length, which limits the validity of the applied correction.

For SDS, the obtained results are in contrast with the previous observation that the reaction proceeds via a two-step mechanism in which the first, adsorption step is selective.²⁹ Rather, we observe that the attraction of diazonium molecules to the SWCNT surface in the initial adsorption step is not necessarily selective but is largely influenced by the surfactant which encapsulates the nanotube. Therefore, selectivity is necessarily imparted in the second step, where electron transfer and covalent bond formation occurs.

Bile Salts: Effects of Surface Packing and Diazonium-Surfactant Interactions. In the case of bile salt-suspended nanotubes, both the structure of the hydrophilic face and the anionic functional group have a significant influence on the reaction behavior of the SWCNT–surfactant complex. These two characteristics alter the SWCNT reactivity by a combination of reagent exclusion effects, which arise due to the dense packing of the adsorbed layer, and diazonium-surfactant coupling, which alters the form of the reactive diazonium species.

With the exception of SC–SWCNTs, the structural packing of the bile salt surfactants on the nanotube surface results in a diameter-dependent reaction in which only a small subset of nanotube species is affected. Among three of the four bile salts that were examined (SDC, STDC, and STC), a similar trend in reactivity is observed, which in all cases results in some degree of quenching of the (10,2), (9,4), and (7,6) fluorescence at 785 nm excitation. This trend is most pronounced in the cases of the deoxycholate bile salts, where a degree of quenching occurs which exceeds 50%. Interestingly, these affected species occupy a narrow range of diameters between $d = 0.88$ and 0.92 nm. The preferential reaction of these nanotubes likely stems from an inability of the surfactant to effectively coat these species,

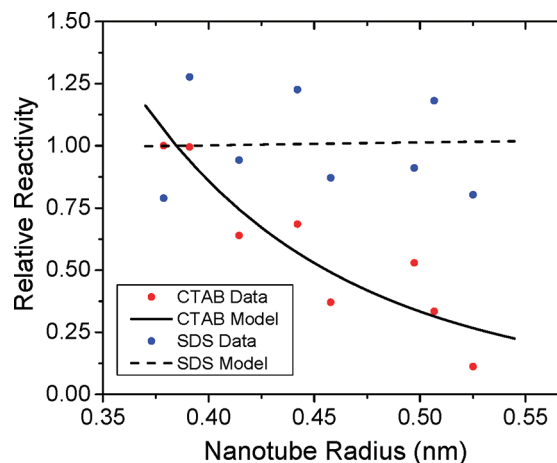


Figure 7. Results of applying a diffusion-limited model to the reaction data for SDS and CTAB. For CTAB, the fitting of the model to experimental data resulted in an estimated surface coverage 4.3 molecules/ nm^2 . For SDS, near-identical trends in reactivity are predicted for a wide range of surface coverages, making it difficult to fit the results to a single value. The black dotted line corresponds to an SDS surface coverage of 2.8 molecules/ nm^2 .

allowing diazonium molecules to access the SWCNT surface. Indeed, it has previously been observed that sodium cholate tends to bind more weakly to the (10,2) nanotube than other chiralities.^{72,73} Here, it is observed that, although the (10,2) chirality exhibits the highest extent of reaction, there is also a significant quenching response among other species with similar diameters. Besides these packing effects, the ionic group of the surfactant also significantly influences the observed reaction trend.

Bile salts that contain carboxylate moieties, such as sodium cholate and sodium deoxycholate, are likely to affect the diazonium-derivatization of carbon nanotubes by altering the reactive diazonium intermediate. This can occur through diazonium-carboxylate coupling, which results in the formation of highly reactive diazoesters.³⁴ The formation of such species is supported by the observation of an enhanced decomposition of aryl diazonium in the case of SDC when compared to a structurally similar bile salt analog, sodium taurodeoxycholate. Because diazoesters have been shown to exhibit an enhanced selectivity toward metallic nanotubes,³⁴ the formation of these intermediates explains the high selectivity of the aryl diazonium ion for metallic species in the case of SC–SWCNT. However, if the carboxylate moiety facilitates diazoester formation, it would also be expected that nanotubes suspended in sodium deoxycholate would demonstrate a similar band gap selective reaction trend, which is not the case. This may be attributed to the formation of secondary micelles around the SWCNT surface, which has been previously proposed for sodium deoxycholate.⁷⁴ In such a case, the secondary layer would assist in maintaining the reactive diazoester at distances greater than those required for electron transfer, and only those species which are poorly coated by the surfactant would predominantly react, which is consistent with experimental results.

Finally, because the reaction of aryl diazonium ions with carbon nanotubes involves electron transfer from the SWCNT to the diazo moiety, we sought to understand the role of the adsorbed layer in stabilizing the diazonium ion near the surface of the nanotube. It has recently been proposed that the selectivity of aryl diazonium ions for metallic species is aided by

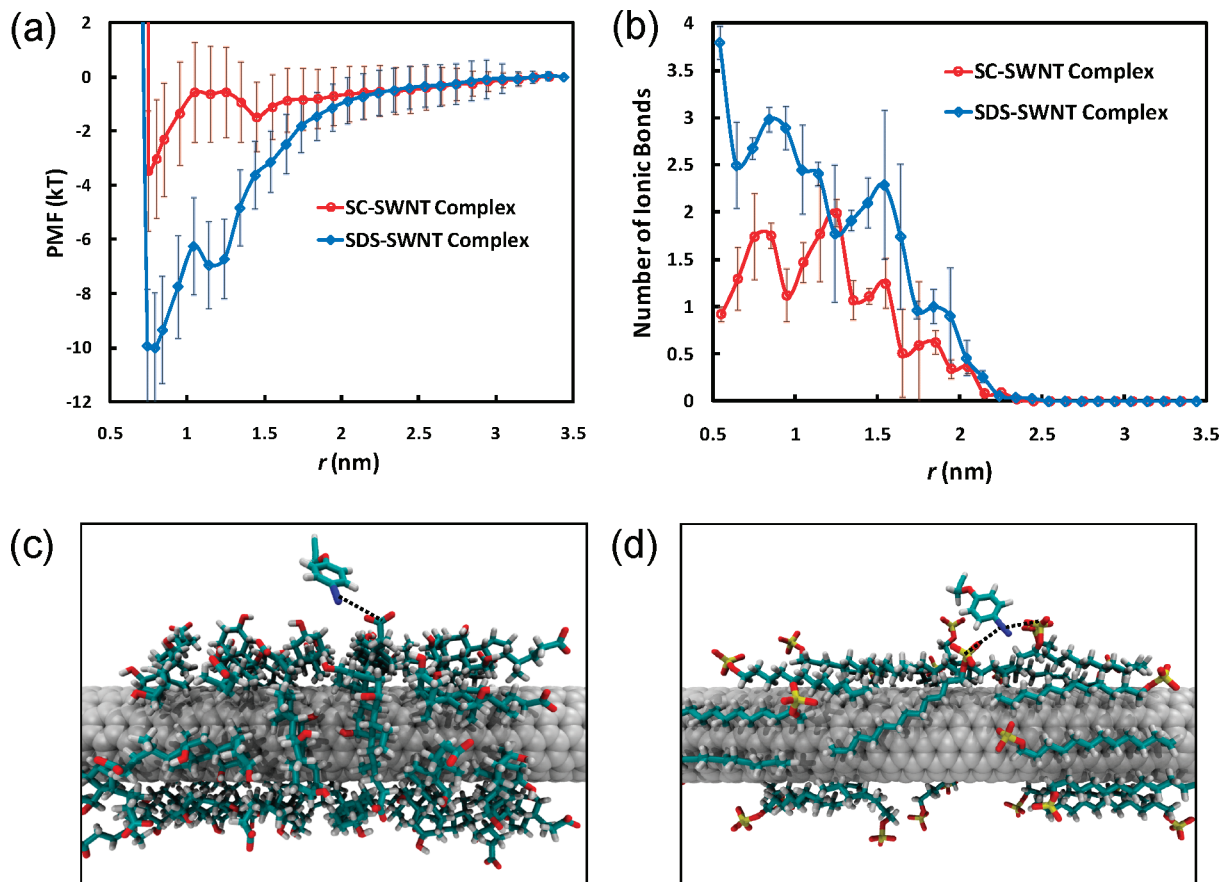


Figure 8. Molecular dynamics simulation results. (a) PMF profile between the diazonium ion and the SWCNT–surfactant complexes for both the SC and the SDS cases. (b) The number of ionic bonds formed between the diazo group and the surfactant head groups. A cutoff distance of 1 nm was used for counting the number of bonds. (c) Simulation snapshots showing the ionic bonds and the cooperative binding between the charged diazo group and the charged surfactant head groups near the SWCNT surface (at $r = 1.5$ nm). Left: SC–SWCNT complex. Right: SDS–SWCNT complex. The black dashed lines denote the ionic bonds. Color code: red, oxygen; light blue, carbon; white, hydrogen; dark blue, nitrogen; gray, carbon in the SWCNT.

a competitive binding between SWCNTs and BF_4^- to donate electron density to the cationic diazo moiety.⁷⁵ Under the assumption that the surfactant layer can play a similar role, we utilized molecular dynamics (MD) simulations to examine the ability of rigid vs linear anionic surfactants to stabilize the aryl diazonium molecule near the surface of the nanotube.

The binding affinity of the diazonium ion in the vicinity of the nanotube surface can be analyzed by evaluating the potential mean force (PMF), acting on the diazonium ion, as a function of the radial distance from the SWCNT surface. The PMF profiles between the diazonium ion and the SWCNT–surfactant complexes are shown in Figure 8a for the cases of both SC and SDS. In general, the long-range electrostatic interaction between the positively charged diazonium ion and the negatively charged SWCNT–surfactant complex facilitates the initial attraction of the diazonium ion to the SWCNT surface. When the diazonium ion approaches the nanotube, the strong van der Waals attraction further enhances the adsorption process, resulting in a global free energy minimum at the SWCNT surface (at $r = 0.75$ nm). As expected, the long-range electrostatic contributions to the PMF profile (for $r \geq 2.5$ nm) between the diazonium ion and the SWCNT–surfactant complex are very similar for the cases of both SC and SDS, which results from the utilization of identical surface charge densities for both systems. However, interestingly, for $r \leq 2.5$ nm, there is a greater increase in the attraction between the aryl

diazonium ion and the SDS–SWCNT complex. This leads to a global free energy well of $-10 \pm 2 k_B T$ in the case of SDS and $-3.5 \pm 2 k_B T$ in the case of SC, which indicates that the binding affinity (reflecting the free energy of adsorption) of the diazonium ion to the SDS–SWCNT complex is much stronger than that of the SC–SWCNT complex.

In order to further investigate the stronger binding affinity between the diazonium ion and the SDS–SWCNT complex, the number of charged surfactant head groups (carboxylates for the SC case and sulfates for the SDS case) around the charged diazonium ion ($-\text{N}^+ \equiv \text{N}$) were evaluated as a function of r (see Figure 8b). These values reflect the number of ionic bonds formed between the diazonium ion and the surfactant head groups. Such interactions are distinct from long-range electrostatic attraction (for $r \geq 2.5$ nm) since they involve a physical connection between the two charged moieties, similar to the formation of salt bridges in the traditional counterion binding phenomenon.⁶⁵ As shown in Figure 8b, there are no ionic bonds for $r \geq 2.5$ nm, since no contacts exist between the diazonium group and the surfactant head groups. However, despite having identical surface coverages, as the aryl diazonium molecule approaches the nanotube surface, there are generally a larger number of ionic bonds formed in the case of SDS–SWCNT when compared to that of SC–SWCNT. Simulation snapshots, which depict this cooperative binding effect, are depicted in Figure 8, panels c and d. In the case of SDS–

SWCNT, the increased number of ionic bonds can be attributed to the fact that the linear, flexible SDS molecules can adjust their positions on the SWCNT surface more easily than the bulkier, rigid SC molecules. Therefore, the rigidity of the sodium cholate molecule ultimately results in a decreased ability of the surfactant to bind, and stabilize the diazonium molecule near the nanotube surface. In addition to surfactant packing effects, such stabilization effects may help to explain why diazonium derivatization occurs much less readily in the case of bile salt reagents when compared to SDS.

CONCLUSIONS

The properties of the surfactant shell have a significant influence on the reactions of aryl diazonium ions with single-walled carbon nanotubes. First, the adsorbed layer, being charged, plays an integral role in defining how the diazonium ion approaches and interacts with the SWCNT–surfactant complex. This is most apparent in the diffusion-limited reactions of linear-chain surfactants, where the charge of the adsorbed layer results in substantially different reaction behavior in the cases of CTAB- and SDS-suspended nanotubes. Here, it was found that, under laser illumination, all species react equivalently in the case of SDS, whereas small diameter species react preferentially in the case of CTAB–SWCNT. The observed small-diameter selectivity of aryl diazonium salts toward CTAB–SWCNTs arises due to diameter-dependent electrostatic effects, which result in a decreased Coulombic barrier to functionalization for smaller nanotubes. Further, these data demonstrate that, contrary to previous findings, the adsorption of diazonium ions onto the SWCNT surface is not necessarily selective but is largely influenced by the surfactant which encapsulates the nanotube. Therefore, selectivity must be imparted in the second step, where electron transfer and covalent bond formation presumably occurs.

Surfactants can also influence the reactions of carbon nanotubes by physically excluding the diazonium ion from the SWCNT surface or by chemically modifying the reactive diazo species. This result was analyzed using four bile salts: sodium cholate, sodium taurocholate, sodium deoxycholate, and sodium taurodeoxycholate. Here, surfactant packing effects result in either very minimal reaction (STC) or reaction among a small population of carbon nanotubes (SDC and STDC), including (10,2), (9,4), (7,6), (10,3), and (11,1). Therefore, especially for the deoxycholate species, it appears to be an inefficiency in surfactant packing, on a narrow range of tube diameters (0.88–0.92 nm), which determines reaction selectivity. In addition, the presence of carboxylate ions on the surfactant appears to facilitate diazoester formation and aryl diazonium decomposition in solution. The formation of such species is likely to be responsible for the highly selective reaction of metallic species in the case of SC–SWCNT.

Structural rigidity can also decrease the ability of the surfactant molecule to stabilize the diazonium ion in the vicinity of the SWCNT surface. Here, molecular dynamics simulations demonstrated that less rigid surfactants are more capable of rearranging on the SWCNT surface, thereby forming a greater number of ionic bonds with the aryl diazonium moiety, and deepening the energy well associated with adsorption. Such results aid in explaining why the reactions of SDS-suspended SWCNTs proceed much more readily than those involving bile salt surfactants and are informative in the design of surfactant–SWCNT complexes that undergo minimal reaction. Such trends offer promise for enhancing the ability to

control the covalent derivatization of carbon nanotubes via careful design of the experimental conditions.

ASSOCIATED CONTENT

S Supporting Information

In depth discussion of model formulation, as well as information on spectral deconvolution and the evaluation of relative reactivities. This material is available free of charge via the Internet at <http://pubs.acs.org>.

AUTHOR INFORMATION

Corresponding Author

*E-mail: strano@mit.edu.

ACKNOWLEDGMENTS

This research is supported in part by the Department of Energy Office of Science Graduate Fellowship Program (DOE SCGF), made possible in part by the American Recovery and Reinvestment Act of 2009, administered by ORISE-ORAU under Contract No. DE-AC05-06OR23100. We also acknowledge funding provided by DuPont through the DuPont-MIT Alliance. Computational resources were partially supported by the Atlantic Computational Excellence Network (ACEnet) in Canada. We thank Prof. Pak Yuet for helpful discussions regarding molecular dynamics simulations.

REFERENCES

- (1) Schnorr, J. M.; Swager, T. M. *Chem. Mater.* **2010**, *23*, 646.
- (2) Kostarelos, K.; Bianco, A.; Prato, M. *Nat. Nano* **2009**, *4*, 627.
- (3) Bianco, A.; Kostarelos, K.; Prato, M. *Curr. Opin. Chem. Biol.* **2005**, *9*, 674.
- (4) Menard-Moyon, C.; Venturelli, E.; Fabbro, C.; Samori, C.; Da Ros, T.; Kostarelos, K.; Prato, M.; Bianco, A. *Expert Opin. Drug Dis.* **2010**, *5*, 691.
- (5) Lin, Y.; Lu, F.; Tu, Y.; Ren, Z. *Nano Lett.* **2003**, *4*, 191.
- (6) Cai, H.; Cao, X.; Jiang, Y.; He, P.; Fang, Y. *Anal. Bioanal. Chem.* **2003**, *375*, 287.
- (7) Zhao, P.; Fang, C. F.; Wang, Y. M.; Zhai, Y. X.; Liu, D. S. *Phys. E* **2009**, *41*, 474.
- (8) Li, X. F.; Wang, L. L.; Chen, K. Q.; Luo, Y. *Appl. Phys. Lett.* **2009**, *95*.
- (9) Sorgenfrei, S.; Chiu, C.-y.; Gonzalez, R. L.; Yu, Y.-J.; Kim, P.; Nuckolls, C.; Shepard, K. L. *Nat Nano* **2011**, *6*, 126.
- (10) Goldsmith, B. R.; Coroneus, J. G.; Khalap, V. R.; Kane, A. A.; Weiss, G. A.; Collins, P. G. *Science* **2007**, *315*, 77.
- (11) Cognet, L.; Tsypbalski, D. A.; Rocha, J. D. R.; Doyle, C. D.; Tour, J. M.; Weisman, R. B. *Science* **2007**, *316*, 1465.
- (12) Siitonen, A. J.; Tsypbalski, D. A.; Bachilo, S. M.; Weisman, R. B. *Nano Lett.* **2010**, *10*, 1595.
- (13) Voiry, D.; Roubeau, O.; Penicaud, A. *J. Mater. Chem.* **2010**, *20*, 4385.
- (14) Brunetti, F. G.; Herrero, M. A.; Munoz, J. D.; Diaz-Ortiz, A.; Alfonsi, J.; Meneghetti, M.; Prato, M.; Vazquez, E. *J. Am. Chem. Soc.* **2008**, *130*, 8094.
- (15) Peng, X. H.; Wong, S. S. *Chem. Mater.* **2009**, *21*, 682.
- (16) Li, X. H.; Niu, J. L.; Zhang, J.; Li, H. L.; Liu, Z. F. *J. Phys. Chem. B* **2003**, *107*, 2453.
- (17) Del Canto, E.; Flavin, K.; Movia, D.; Navio, C.; Bittencourt, C.; Giordani, S. *Chem. Mater.* **2010**, *23*, 67.
- (18) Bachilo, S. M.; Strano, M. S.; Kittrell, C.; Hauge, R. H.; Smalley, R. E.; Weisman, R. B. *Science* **2002**, *298*, 2361.
- (19) Singh, P.; Campidelli, S.; Giordani, S.; Bonifazi, D.; Bianco, A.; Prato, M. *Chem. Soc. Rev.* **2009**, *38*, 2214.
- (20) Banerjee, S.; Wong, S. S. *J. Am. Chem. Soc.* **2004**, *126*, 2073.

- (21) Strano, M. S.; Dyke, C. A.; Usrey, M. L.; Barone, P. W.; Allen, M. J.; Shan, H. W.; Kittrell, C.; Hauge, R. H.; Tour, J. M.; Smalley, R. E. *Science* **2003**, *301*, 1519.
- (22) Graupner, R.; Abraham, J.; Wunderlich, D.; Vencelová, A.; Lauffer, P.; Röhrl, J.; Hundhausen, M.; Ley, L.; Hirsch, A. *J. Am. Chem. Soc.* **2006**, *128*, 6683.
- (23) Li, J. Q.; Jia, G. X.; Zhang, Y. F.; Chen, Y. *Chem. Mater.* **2006**, *18*, 3579.
- (24) Bahr, J. L.; Yang, J.; Kosynkin, D. V.; Bronikowski, M. J.; Smalley, R. E.; Tour, J. M. *J. Am. Chem. Soc.* **2001**, *123*, 6536.
- (25) Graff, R. A.; Swanson, T. M.; Strano, M. S. *Chem. Mater.* **2008**, *20*, 1824.
- (26) Li, H. M.; Cheng, F. O.; Duft, A. M.; Adronov, A. *J. Am. Chem. Soc.* **2005**, *127*, 14518.
- (27) Patai, S. *The Chemistry of diazonium and diazo groups*; J. Wiley: New York, 1978.
- (28) Doyle, C. D.; Rocha, J. D. R.; Weisman, R. B.; Tour, J. M. *J. Am. Chem. Soc.* **2008**, *130*, 6795.
- (29) Usrey, M. L.; Lippmann, E. S.; Strano, M. S. *J. Am. Chem. Soc.* **2005**, *127*, 16129.
- (30) Schmidt, G.; Gallon, S.; Esnouf, S.; Bourgoin, J. P.; Chenevier, P. *Chem.—Eur. J.* **2009**, *15*, 2101.
- (31) Nair, N.; Kim, W. J.; Usrey, M. L.; Strano, M. S. *J. Am. Chem. Soc.* **2007**, *129*, 3946.
- (32) Kim, W. J.; Usrey, M. L.; Strano, M. S. *Chem. Mater.* **2007**, *19*, 1571.
- (33) Kim, W. J.; Nair, N.; Lee, C. Y.; Strano, M. S. *J. Phys. Chem. C* **2008**, *112*, 7326.
- (34) Schmidt, G.; Filoromo, A.; Derycke, V.; Bourgoin, J.-P.; Chenevier, P. *Chem.—Eur. J.* **2011**, *17*, 1415.
- (35) Liu, J.; An, L.; Fu, Q. A.; Lu, C. G. *J. Am. Chem. Soc.* **2004**, *126*, 10520.
- (36) Burghard, M.; Balasubramanian, K.; Sordan, R.; Kern, K. *Nano Lett.* **2004**, *4*, 827.
- (37) Israelachvili, J. N. *Intermolecular and surface forces*, 3rd ed.; Academic Press: Burlington, MA, 2011.
- (38) Weizmann, Y.; Lim, J.; Chenoweth, D. M.; Swager, T. M. *Nano Lett.* **2010**, *10*, 2466.
- (39) Weizmann, Y.; Chenoweth, D. M.; Swager, T. M. *J. Am. Chem. Soc.* **2010**, *132*, 14009.
- (40) Piran, M.; Kotlyar, V.; Medina, D. D.; Pirlot, C.; Goldman, D.; Lellouche, J. P. *J. Mater. Chem.* **2009**, *19*, 631.
- (41) O'Connell, M. J.; Bachilo, S. M.; Huffman, C. B.; Moore, V. C.; Strano, M. S.; Haroz, E. H.; Rialon, K. L.; Boul, P. J.; Noon, W. H.; Kittrell, C.; Ma, J. P.; Hauge, R. H.; Weisman, R. B.; Smalley, R. E. *Science* **2002**, *297*, 593.
- (42) Jin, Z.; McNicholas, T. P.; Shih, C.-J.; Wang, Q. H.; Paulus, G. L. C.; Hilmer, A. J.; Shimizu, S.; Strano, M. S. *Chem. Mater.* **2011**, *23*, 3362.
- (43) Seyed, S. M.; Jafari, Z.; Attaran, N.; Sadeghian, H.; Saberi, M. R.; Riazi, M. M. *Bioorg. Med. Chem.* **2009**, *17*, 1614.
- (44) Barone, P. W.; Yoon, H.; Ortiz-Garcia, R.; Zhang, J. Q.; Ahn, J. H.; Kim, J. H.; Strano, M. S. *ACS Nano* **2009**, *3*, 3869.
- (45) Hess, B.; Kutzner, C.; van der Spoel, D.; Lindahl, E. *J. Chem. Theory Comput.* **2008**, *4*, 435.
- (46) Lin, S. C.; Blankschtein, D. *J. Phys. Chem. B* **2010**, *114*, 15616.
- (47) Jorgensen, W. L.; Maxwell, D. S.; Tirado-Rives, J. *J. Am. Chem. Soc.* **1996**, *118*, 11225.
- (48) Jorgensen, W. L.; Price, M. L. P.; Ostrovsky, D. *J. Comput. Chem.* **2001**, *22*, 1340.
- (49) Lopes, J. N. C.; Padua, A. A. H.; Shimizu, K. *J. Phys. Chem. B* **2008**, *112*, 5039.
- (50) Frisch, M. J.; Trucks, G. W.; Schlegel, H. B.; Scuseria, G. E.; Robb, M. A.; Cheeseman, J. R.; Montgomery, J. A.; Vreven, T.; Kudin, K. N.; Burant, J. C.; Millam, J. M.; Iyengar, S. S.; Tomasi, J.; Barone, V.; Mennucci, B.; Cossi, M.; Scalmani, G.; Rega, N.; Petersson, G. A.; Nakatsuji, H.; Hada, M.; Ehara, M.; Toyota, K.; Fukuda, R.; Hasegawa, J.; Ishida, M.; Nakajima, T.; Honda, Y.; Kitao, O.; Nakai, H.; Klene, M.; Li, X.; Knox, J. E.; Hratchian, H. P.; Cross, J. B.; Bakken, V.; Adamo, C.; Jaramillo, J.; Gomperts, R.; Stratmann, R. E.; Yazyev, O.; Austin, A. J.; Cammi, R.; Pomelli, C.; Ochterski, J. W.; Ayala, P. Y.; Morokuma, K.; Voth, G. A.; Salvador, P.; Dannenberg, J. J.; Zakrzewski, V. G.; Dapprich, S.; Daniels, A. D.; Strain, M. C.; Farkas, O.; Malick, D. K.; Rabuck, A. D.; Raghavachari, K.; Foresman, J. B.; Ortiz, J. V.; Cui, Q.; Baboul, A. G.; Clifford, S.; Cioslowski, J.; Stefanov, B. B.; Liu, G.; Liashenko, A.; Piskorz, P.; Komaromi, I.; Martin, R. L.; Fox, D. J.; Keith, T.; Laham, A.; Peng, C. Y.; Nanayakkara, A.; Challacombe, M.; Gill, P. M. W.; Johnson, B.; Chen, W.; Wong, M. W.; Gonzalez, C.; Pople, J. A. *Gaussian 03*, revision C.02; Gaussian, Inc.: Wallingford, CT, 2003.
- (51) Breneman, C. M.; Wiberg, K. B. *J. Comput. Chem.* **1990**, *11*, 361.
- (52) Lopes, J. N. C.; Deschamps, J.; Padua, A. A. H. *J. Phys. Chem. B* **2004**, *108*, 2038.
- (53) Lopes, J. N. C.; Padua, A. A. H. *J. Phys. Chem. B* **2004**, *108*, 16893.
- (54) Dunning, T. H. *J. Chem. Phys.* **1989**, *90*, 1007.
- (55) Schuchardt, K. L.; Didier, B. T.; Elsethagen, T.; Sun, L. S.; Gurumoorthi, V.; Chase, J.; Li, J.; Windus, T. L. *J. Chem. Inf. Model.* **2007**, *47*, 1045.
- (56) Feller, D. *J. Comput. Chem.* **1996**, *17*, 1571.
- (57) Richard, C.; Balavoine, F.; Schultz, P.; Ebbesen, T. W.; Mioskowski, C. *Science* **2003**, *300*, 775.
- (58) Striolo, A.; Tummala, N. R. *ACS Nano* **2009**, *3*, 595.
- (59) Yang, X. N.; Xu, Z. J.; Yang, Z. *Nano Lett.* **2010**, *10*, 985.
- (60) Mukhopadhyay, S.; Maitra, U. *Curr. Sci. India* **2004**, *87*, 1666.
- (61) Hilmer, A. J.; Nair, N.; Strano, M. S. *Nanotechnology* **2010**, *21*, 495703.
- (62) Vlachy, V. *Annu. Rev. Phys. Chem.* **1999**, *50*, 145.
- (63) Borukhov, I. *J. Polym. Sci. Polym. Phys.* **2004**, *42*, 3598.
- (64) Siitonen, A. J.; Tsypbalski, D. A.; Bachilo, S. M.; Weisman, R. B. *J. Phys. Chem. Lett.* **2010**, *1*, 2189.
- (65) Hiemenz, P. C.; Rajagopalan, R. *Principles of colloid and surface chemistry*, 3rd ed.; Marcel Dekker: New York, 1997.
- (66) Borukhov, I.; Andelman, D.; Orland, H. *Phys. Rev. Lett.* **1997**, *79*, 435.
- (67) D'Angelo, P.; Migliorati, V.; Guidoni, L. *Inorg. Chem.* **2010**, *49*, 4224.
- (68) Raugei, S.; Klein, M. L. *J. Chem. Phys.* **2002**, *116*, 196.
- (69) Ricci, M. A.; Mancinelli, R.; Botti, A.; Bruni, F.; Soper, A. K. *J. Phys. Chem. B* **2007**, *111*, 13570.
- (70) White, J. A.; Schwegler, E.; Galli, G.; Gygi, F. *J. Chem. Phys.* **2000**, *113*, 4668.
- (71) Grossjord, N.; van der Schoot, P.; Meuldijk, J.; Koning, C. E. *Langmuir* **2007**, *23*, 3646.
- (72) McDonald, T. J.; Engtrakul, C.; Jones, M.; Rumbles, G.; Heben, M. J. *J. Phys. Chem. B* **2006**, *110*, 25339.
- (73) McDonald, T. J.; Blackburn, J. L.; Metzger, W. K.; Rumbles, G.; Heben, M. J. *J. Phys. Chem. C* **2007**, *111*, 17894.
- (74) Bonaccorso, F.; Hasan, T.; Tan, P. H.; Sciascia, C.; Privitera, G.; Di Marco, G.; Gucciardi, P. G.; Ferrari, A. C. *J. Phys. Chem. C* **2010**, *114*, 17267.
- (75) Sumpter, B. G.; Jiang, D.-E.; Meunier, V. *Small* **2008**, *4*, 2035.